Finite-Temperature Mott Transition in Two-Dimensional Frustrated Hubbard Models

Takuma Ohashi [1,2], Tsutomu Momoi [2], Hirokazu Tsunetsugu [3] and Norio Kawakami [4]

[1]*Department of Physics, Osaka University, Toyonaka, Osaka 560-0043, Japan.*
[2]*Condensed Matter Theory Laboratory, RIKEN, Wako, Saitama 351-0198, Japan.*
[3]*Institute for Solid State Physics, University of Tokyo, Kashiwa, Chiba 277-8581, Japan.*
[4]*Department of Physics, Kyoto University, Kyoto 606-8502, Japan*

We investigate the Hubbard model on two typical frustrated lattices in two dimensions, the kagomé lattice and the anisotropic triangular lattice, by means of the cellular dynamical mean field theory. We show that the metallic phase is stabilized up to fairly large Hubbard interactions under strong geometrical frustration in both cases, which results in heavy fermion behavior and several anomalous properties around the Mott transition point. In particular, for the anisotropic triangular lattice, we find novel reentrant behavior in the Mott transition in the moderately frustrated parameter regime, which is caused by the competition between Fermi-liquid formation and magnetic correlations. It is demonstrated that the reentrant behavior is a generic feature inherent in the Mott transition with intermediate geometrical frustration, and indeed in accordance with recent experimental findings for organic materials.

§1. Introduction

Geometrical frustration has attracted much interest in strongly correlated electron systems. Among a number of intriguing phenomena, the observation of heavy fermion behavior in LiV_2O_4[1),2)] with the pyrochlore lattice structure has activated theoretical studies of electron correlations with geometrical frustration. Also, the discovery of superconductivity in the triangular-lattice oxide $Na_xCoO_2 \cdot yH_2O$[3)] and the β-pyrochlore osmate AOs_2O_6 (A =K,[4)] Rb,[5)] Cs[6)]) has stimulated further investigations of frustrated electron systems. These intensive studies have revealed new aspects of the Mott transition for geometrically frustrated electrons. In particular, an experimental demonstration of the spin liquid ground state in the Mott insulating phase in the organic material κ-(BEDT-TTF)$_2$Cu$_2$CN$_3$[7)] with triangular lattice structure, raises a theoretical challenge in the physics of geometrically frustrated electron systems. Other materials found recently, such as the pyrochlore Kondo lattice compound $Pr_2Ir_2O_7$[8)] and the hyperkagomé compound $Na_4Ir_3O_8$,[9)] also provide new examples of frustrated electron systems with nonmagnetic ground state. In this paper, we will investigate the two fundamental frustrated systems, the kagomé lattice and the anisotropic triangular lattice, which we will briefly explain below.

1.1. *Kagomé lattice*

The kagomé lattice is one of typical frustrated systems and it shares some essential properties of the pyrochlore lattice. Antiferromagnetic spin systems on

this lattice have been intensively studied and many unusual properties have been found.[10),11)] Theoretical studies of the $S = 1/2$ Heisenberg antiferromagnet has suggested the realization of a nonmagnetic ground state and the existence of anomalous singlet excitations within the singlet-triplet gap due to strong frustration. Therefore, it is natural to ask what kind of quasiparticle dynamics these unusual properties induce if electrons become itinerant. An interesting example of the itinerant kagomé systems may be a superconducting compound $Na_xCoO_2 \cdot yH_2O$. It has been suggested that an effective model of this material can be regarded as a correlated electron system on the kagomé lattice by properly considering anisotropic hopping matrix elements of the cobalt $3d$ orbitals.[12)] Also, the hyperkagomé compound $Na_4Ir_3O_8$ is a three dimensional analog of the kagomé lattice electron system. The issue of electron correlations for the kagomé lattice was addressed recently in the studies by using the fluctuation-exchange (FLEX) approximation[13)] and quantum Monte Carlo (QMC) method.[14)] These studies focused on electron correlations in the metallic regime, and the nature of the Mott transition has not been clarified. We shall investigate in this paper the kagomé lattice electron system with particular emphasis on the Mott transition under the influence of strong frustration.

1.2. *Triangular lattice*

Another remarkable example is a triangular electron system with strong correlations, in which the metal-insulator transition has intensively studied. This has particularly been stimulated by various interesting phenomena recently found in organic materials κ-(BEDT-TTF)$_2X$ around the Mott transition, such as a spin liquid state, unconventional superconductivity, etc.[7),15),16)] A possible nonmagnetic ground state is found in the triangular lattice Hubbard model by the path integral renormalization group study, which provides a powerful numerical treatment of the frustrated electron systems,[17)] and the correlated electrons on the anisotropic triangular lattice have been intensively studied so far.[18)–27)] The effects of geometrical frustration on finite-temperature (T) Mott transition, however, have not yet been sufficiently understood. One of the interesting and nontrivial features of the finite-T Mott transition is a reentrant behavior observed in the frustrated organic material κ-(BEDT-TTF)$_2$Cu[N(CN)$_2$]Cl under pressure.[15),16)] With lowering temperature, it once undergoes a transition from Mott insulator to metal, and then reenters the paramagnetic insulating phase at a much lower temperature. This reentrant behavior is quite different from the nonreentrant behavior of Mott transition in the three dimensional systems, such as V_2O_3, and is expected to be a new aspect of the geometrical frustration and possibly low-dimensionality. We will address this problem in this paper.

1.3. *Theoretical approach*

In order to investigate the Mott transition in the kagomé and triangular electron systems, we need advanced theoretical methods. Among many approaches for correlated electron systems, the dynamical mean field theory (DMFT)[28)–30)] has given substantial theoretical progress in understanding the Mott transition,[31)] and it has also clarified various interesting phenomena[29),32)] in the strongly correlated electron

systems, such as magnetism,[33)–39)] heavy fermion formation,[40)–45)] orbital physics in the multiband systems,[46)–54)] etc. Recently, DMFT has been also applied to cold atoms in an optical lattice,[55)–58)] some inhomogeneous systems,[59)–61)] and photo-excited semiconductors.[62),63)] However, DMFT does not take account of spatially extended correlations, which should be included for the systems under consideration in this paper. Therefore, it is desirable to study the Mott transition by employing another appropriate method which properly incorporate spatially extended correlations and geometrical frustration. Cluster extensions of DMFT[64)–68)] or the self energy functional approach[70)] are candidates for this purpose. Recently developed diagrammatic extensions of DMFT[71),72)] might also treat geometrical frustration by incorporating the **k**-dependence of the self-energy. Here we will use a cluster extension of DMFT, the cellular dynamical mean field theory (CDMFT).[65),66)]

1.4. *Purpose of the paper*

In this paper, we give a brief review of our recent studies on the Mott transitions in the Hubbard model on the geometrically frustrated kagomé[73)–75)] and anisotropic triangular lattices[76)] by means of CDMFT combined with QMC.[77)] We investigate these models separately to discuss properties characteristic of each system, and then deduce common properties inherent in frustrated electron systems. In both models, we find that the metallic phase is stable up to fairly large Hubbard interactions under strong geometrical frustration, giving rise to the heavy fermion behavior near the Mott transition. In the kagomé lattice, several anomalous properties of spin correlation functions, such as nonmonotonic temperature dependence, emerge around the Mott transition. For the anisotropic triangular lattice, we discover more striking behavior in the Mott transition. Namely, in moderately frustrated cases, the finite-T Mott transition shows a reentrant behavior, which is consistent with experiments in some organic materials.[15),16)] We demonstrate that the reentrant behavior is a characteristic feature inherent in the Mott transition with geometrical frustration, and thus can be experimentally observed in various frustrated electron systems.

The paper is organized as follows. In the next section, we introduce the model Hamiltonian and briefly explain the framework of CDMFT. We first study the Mott transition in the kagomé lattice Hubbard model and elucidate some anomalous properties appearing near the transition point in §3. In §4, we then investigate the reentrant Mott transition on the anisotropic triangular lattice. A brief summary is given in the last section.

§2. Model and method

We consider the standard Hubbard model on the kagomé lattice (see Fig. 2(a)) and the anisotropic triangular lattice (see Fig. 13),

$$H = \sum_{i,j,\sigma} t_{ij} c^{\dagger}_{i\sigma} c_{j\sigma} + U \sum_{i} n_{i\uparrow} n_{i\downarrow}, \tag{2·1}$$

with $n_{i\sigma} = c^{\dagger}_{i\sigma} c_{i\sigma}$, where $c^{\dagger}_{i\sigma}$ ($c_{i\sigma}$) creates (annihilates) an electron with spin σ at site i. Here, $i, j = 1, 2, \cdots, N$, and N is the total number of sites. The hopping matrix

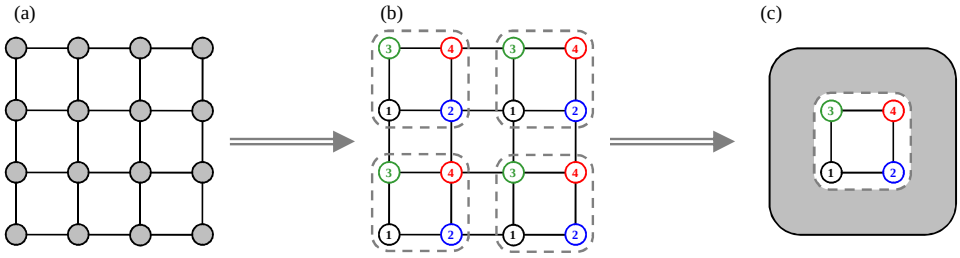

Fig. 1. (Color online) Sketch of the original lattice (a), superlattice (b) and effective cluster model (c) for the cluster size $N_c = 4$.

element and the Hubbard interaction are denoted as t_{ij} and U, respectively. The explicit form of t_{ij} will be given for each model below. Note that in both models, a triangular structure of the unit cell, which is a source of strong frustration, plays a crucial role in controlling the nature of Mott transition. Therefore, theoretical methods beyond DMFT are necessary to incorporate spatially extended electron correlations. To this end, we here use CDMFT, which has been successfully applied to frustrated systems such as the Hubbard model on the triangular lattice[21),24),25)] and the kagomé lattice.[73)]

2.1. *Cellular dynamical mean field theory*

In CDMFT, the original lattice is regarded as a superlattice consisting of small clusters, as shown in Fig. 1 (b). Here, we define the cluster size as N_c. The model (2·1) is rewritten as,

$$H = \sum_{l,m,\gamma,\delta,\sigma} t_{\gamma,\delta}\left(l,m\right) c^{\dagger}_{l\gamma\sigma} c_{m\delta\sigma} + U \sum_{l,\gamma} n_{l\gamma\uparrow} n_{l\gamma\downarrow}, \tag{2·2}$$

where l and m are cluster indices, $l, m = 1, 2, \cdots, N/N_c$, and γ and δ are sublattice indices, $\gamma, \delta = 1, 2, \cdots, N_c$. Using a standard DMFT procedure with the inter-cluster hopping scaled as $t_{\gamma,\delta}(l,m) \to t_{\gamma,\delta}(l,m)/\sqrt{d}$, the original model is then mapped onto an effective cluster model consisting of a cluster coupled to the self-consistently determined medium, as illustrated in Fig. 1 (c). The corresponding action reads

$$\begin{aligned} S_{\text{eff}} = & \int_0^{\beta} d\tau \int_0^{\beta} d\tau' \sum_{\gamma,\delta,\sigma} c^{\dagger}_{\gamma\sigma}\left(\tau\right) \left(\mathcal{G}^{-1}\right)_{\gamma\delta\sigma}\left(\tau-\tau'\right) c_{\delta\sigma}\left(\tau'\right) \\ & + U \int_0^{\beta} d\tau \sum_{\gamma} n_{\gamma\uparrow}\left(\tau\right) n_{\gamma\downarrow}\left(\tau\right). \end{aligned} \tag{2·3}$$

Here, $\beta = 1/T$. Given the Green's function for the effective medium, $\hat{\mathcal{G}}_{\sigma}$, we can compute the cluster Green's function $\hat{G}_{\sigma}$ by solving the effective cluster model with QMC method,[77)] and then we obtain the cluster self-energy $\hat{\Sigma}_{\sigma}$. Here, $\hat{\mathcal{G}}_{\sigma}$, $\hat{G}_{\sigma}$, and $\hat{\Sigma}_{\sigma}$ are $N_c \times N_c$ matrices. In order to reduce errors due to finite time slices in QMC, we exploit an interpolation scheme based on a high-frequency expansion of the discrete imaginary-time Green's function.[78)] The effective medium $\hat{\mathcal{G}}_{\sigma}$ is then

updated by the Dyson equation,

$$\hat{\mathcal{G}}_\sigma^{-1}\left(i\omega_n\right) = \left[\frac{N_c}{N}\sum_{\tilde{\mathbf{k}}}\hat{g}_\sigma\left(\tilde{\mathbf{k}} : i\omega_n\right)\right]^{-1} + \hat{\Sigma}_\sigma\left(i\omega_n\right), \tag{2·4}$$

$$\hat{g}_\sigma\left(\tilde{\mathbf{k}} : i\omega_n\right) = \left[i\omega_n + \mu - \hat{t}\left(\tilde{\mathbf{k}}\right) - \hat{\Sigma}_\sigma\left(i\omega_n\right)\right]^{-1}, \tag{2·5}$$

where μ is the chemical potential and $\hat{t}(\tilde{\mathbf{k}})$ is the Fourier-transformed hopping matrix for the superlattice,

$$t_{\gamma\delta}\left(\tilde{\mathbf{k}}\right) = \frac{N_c}{N}\sum_{l,m} e^{-\tilde{\mathbf{k}}\cdot\left(\mathbf{r}_l - \mathbf{r}_m\right)} t_{\gamma\delta}\left(l,m\right). \tag{2·6}$$

Here the summation of $\tilde{\mathbf{k}}$ is taken over the reduced Brillouin zone of the superlattice.

2.2. *Wave-vector dependent properties*

Within CDMFT, the single-electron Green's function for wave vector $\mathbf{k}$ is given as,

$$G_{\mathbf{k}}\left(i\omega_n\right) = \frac{1}{N_c}\sum_{\gamma,\delta} e^{i\mathbf{k}\cdot\left(\mathbf{r}_\gamma - \mathbf{r}_\delta\right)}\left[i\omega_n + \mu - \hat{t}\left(\mathbf{k}\right) - \hat{\Sigma}\left(i\omega_n\right)\right]^{-1}_{\gamma\delta}, \tag{2·7}$$

where $\mathbf{k}$ is the wave vector in the original Brillouin zone and $\mathbf{r}_\gamma$, $\mathbf{r}_\delta$ label cluster sites.[69] We calculate the imaginary time Green's function $G_{\mathbf{k}}(\tau)$ and obtain the spectrum $A_{\mathbf{k}}(\omega) = -\mathrm{Im}G_{\mathbf{k}}(\omega + i0)/\pi$ using the maximum entropy method (MEM).[80]

It is also possible to compute the wave-vector dependence of various two-electron Green's functions with including vertex corrections. Here, we investigate the $\mathbf{q}$-dependent static spin susceptibility defined as,

$$\chi_{\gamma\delta}(\tilde{\mathbf{q}}) = \frac{N_c}{N}\int_0^\beta d\tau \sum_{\tilde{\mathbf{k}},\tilde{\mathbf{k}}'}\left\langle c^\dagger_{\tilde{\mathbf{k}}\gamma\uparrow}\left(\tau\right) c_{\tilde{\mathbf{k}}+\tilde{\mathbf{q}}\gamma\downarrow}\left(\tau\right) c^\dagger_{\tilde{\mathbf{k}}'+\tilde{\mathbf{q}}\delta\downarrow}\left(0\right) c_{\tilde{\mathbf{k}}'\delta\uparrow}\left(0\right)\right\rangle. \tag{2·8}$$

In order to incorporate the vertex correction into the susceptibility, we consider the two-electron Green's function in the effective cluster model (2·3),

$$C_{\gamma\delta}\left(i\omega_l, i\omega_m\right) = \frac{1}{\beta}\int_0^\beta\int_0^\beta\int_0^\beta\int_0^\beta d\tau_1 d\tau_2 d\tau_3 d\tau_4 \times e^{-i\omega_l\left(\tau_1-\tau_2\right)} e^{-i\omega_m\left(\tau_3-\tau_4\right)} C_{\gamma\delta}\left(\tau_1,\tau_2,\tau_3,\tau_4\right), \tag{2·9}$$

$$C_{\gamma\delta}\left(\tau_1,\tau_2,\tau_3,\tau_4\right) = \left\langle \mathrm{T}_\tau c^\dagger_{\gamma\uparrow}\left(\tau_1\right) c_{\gamma\downarrow}\left(\tau_2\right) c^\dagger_{\delta\downarrow}\left(\tau_3\right) c_{\delta\uparrow}\left(\tau_4\right)\right\rangle. \tag{2·10}$$

We first calculate the cluster two-electron Green's function (2·10) by QMC and extract the vertex function $\Gamma_{\gamma\delta}\left(i\omega_l, i\omega_m\right)$ via the Bethe-Salpeter equation,

$$\hat{\Gamma} = \hat{C^0}^{-1} - \hat{C}^{-1}, \tag{2·11}$$

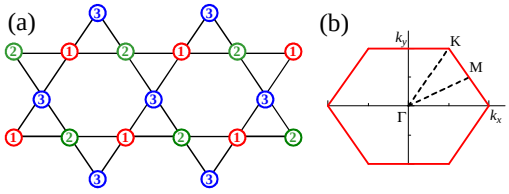

Fig. 2. (Color online) (a) Sketch of the kagomé lattice and (b) the first Brillouin zone.

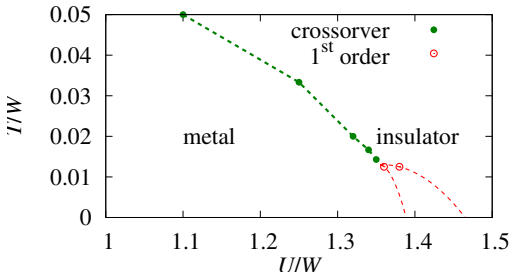

Fig. 3. (Color online) Phase diagram of the kagomé lattice Hubbard model. The dashed lines are guide to eye.

where C^0 is the bare cluster two-electron Green's function,

$$C^0_{\gamma\delta}(i\omega_l, i\omega_m) = -\beta \left[\frac{N_c}{N}\sum_{\tilde{\mathbf{k}}} g_{\gamma\delta\downarrow}\left(\tilde{\mathbf{k}} : i\omega_l\right)\right]\left[\frac{N_c}{N}\sum_{\tilde{\mathbf{k}}} g_{\delta\gamma\uparrow}\left(\tilde{\mathbf{k}} : i\omega_l\right)\right]\delta_{l,m}. \quad (2\cdot12)$$

Here, $\hat{C}^0$, $\hat{C}$ and $\hat{\Gamma}$ are $N_cN_f \times N_cN_f$ matrices, and N_f is the number of the Matsubara frequency. On the other hand, the bare two-electron Green's function in the lattice system is calculated as,

$$C^0_{\gamma\delta}(\tilde{\mathbf{q}} : i\omega_l, i\omega_m) = -\frac{\beta N_c}{N}\sum_{\tilde{\mathbf{k}}} g_{\gamma\delta\downarrow}\left(\tilde{\mathbf{k}}+\tilde{\mathbf{q}} : i\omega_l\right) g_{\gamma\delta\uparrow}\left(\tilde{\mathbf{k}} : i\omega_l\right)\delta_{l,m}. \quad (2\cdot13)$$

By using Eqs. (2·11) and (2·13), we can compute the lattice two-electron Green's function,

$$\hat{C}\left(\tilde{\mathbf{q}}\right) = \left[\hat{C^0}\left(\tilde{\mathbf{q}}\right)^{-1} - \hat{\Gamma}\right]^{-1}. \quad (2\cdot14)$$

Taking account of the phase factor, we finally obtain the $\mathbf{q}$-dependent susceptibility,

$$\chi_{\gamma\delta}(\tilde{\mathbf{q}}) = \frac{1}{\beta^2}\sum_{l,m} C_{\gamma\delta}\left(\tilde{\mathbf{q}} : i\omega_l, i\omega_m\right) e^{-i\tilde{\mathbf{q}}\cdot(\mathbf{r}_\gamma - \mathbf{r}_\delta)}. \quad (2\cdot15)$$

§3. Kagomé lattice system

In this section, we investigate the Mott transition in the kagomé lattice Hubbard model by means of CDMFT and determine the phase diagram for the Mott transition. The result is shown in Fig. 3.

Let us consider the Hubbard model (2·1) with nearest-neighbor hopping on the kagomé lattice (see Fig. 2 (a)),

$$t_{ij} = \begin{cases} -t & (t>0) \quad (\text{site } i \text{ an } j: \text{ nearest neighbors}) \\ 0 & (\text{otherwise}) \end{cases}. \quad (3\cdot1)$$

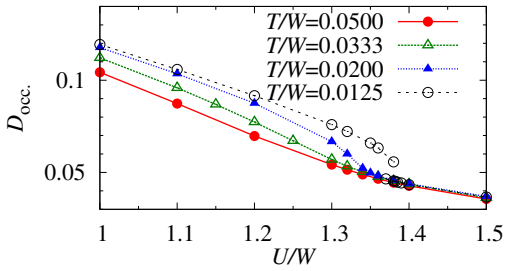

Fig. 4. (Color online) Double occupancy as a function of interaction strength U/W. At $T/W = 0.0125$, we can see the discontinuity with hysteresis, indicating the first-order Mott transition.

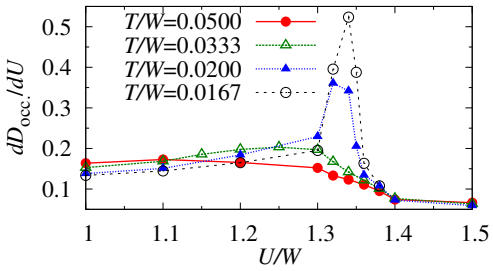

Fig. 5. (Color online) Derivatives of double occupancy $dD_{\mathrm{occ.}}/dU$. We define the crossover point U^* in the phase diagram Fig. 3 by U that gives a maximum of $dD_{\mathrm{occ.}}/dU$.

The band width is $W = 6t$ and we will use it as an energy unit. Unit cell of the kagomé lattice has three sites and they are labeled by 1, 2, and 3, as shown in Fig. 2(a). We choose this unit cell as a cluster for the CDMFT approach and map the system to an effective cluster model. Self-consistent solution of self-energy matrix is obtained by means of iterative procedure explained in the previous section, and twenty-times iterations are sufficient to achieve satisfactory convergence. In each iteration, the local single- and two-electron Green's function for the effective model are calculated by QMC, where we typically use 10^6 QMC sweeps and Trotter time slices $L = 2W\beta$ to reach sufficient computational accuracy.

3.1. *Mott transition*

We now investigate the Mott transition at half filling. Figure 4 shows U-dependence of the double occupancy $D_{\mathrm{occ.}} = \langle n_{i\uparrow} n_{i\downarrow} \rangle$ for several choices of temperature. At high temperatures, $D_{\mathrm{occ.}}$ smoothly decreases as U increases, which indicates that local spin moments are developed. As the temperature is lowered, a singular behavior emerges around characteristic values of U. When $0.014 \leq T/W \leq 0.05$, $D_{\mathrm{occ.}}$ shows a crossover around $U/W \sim 1.0$-1.4. For reference, in Fig. 5, we show $dD_{\mathrm{occ.}}/dU$, which is computed by numerical differentiation of $D_{\mathrm{occ.}}$. The maximum of $dD_{\mathrm{occ.}}/dU$ can be identified as the metal-insulator crossover. Therefore, we define the crossover point U^* by U that gives a maximum of $dD_{\mathrm{occ.}}/dU$. At lower temperature $T/W = 0.0125$, the crossover evolves to a discontinuity accompanied by hysteresis, which characterizes a first-order phase transition at $U_c/W \sim 1.37$. We thus end up with the phase diagram shown in Fig. 3, where the critical end point is located at $U/W \sim 1.36$ and $T/W \sim 0.014$. We note that U_c is much larger than the crossover strength of U found for the unfrustrated square lattice model.[79] As is the case for the triangular lattice,[21] the double occupancy $D_{\mathrm{occ.}}$ increases in the metallic phase ($U < U_c$) as T decreases, while it is almost independent of T in the insulating phase ($U > U_c$). The increase of $D_{\mathrm{occ.}}$ at low temperatures implies that local moments are suppressed due to the itinerancy of electrons, which in turn leads to the development of coherent quasiparticle dynamics. It should be noticed that in the metallic phase near the critical point, $D_{\mathrm{occ.}}$ starts to increase at very

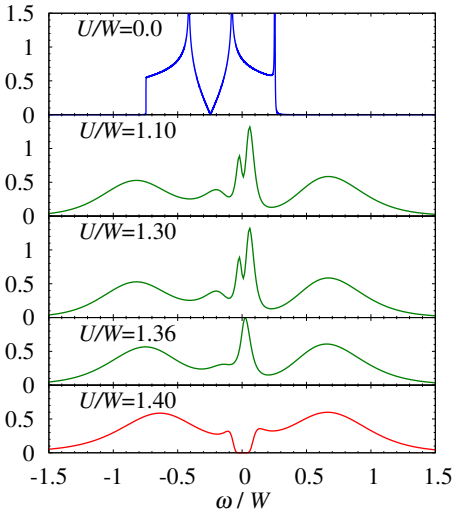

Fig. 6. (Color online) Density of states at $T/W = 0.0125$ for several values of U/W.

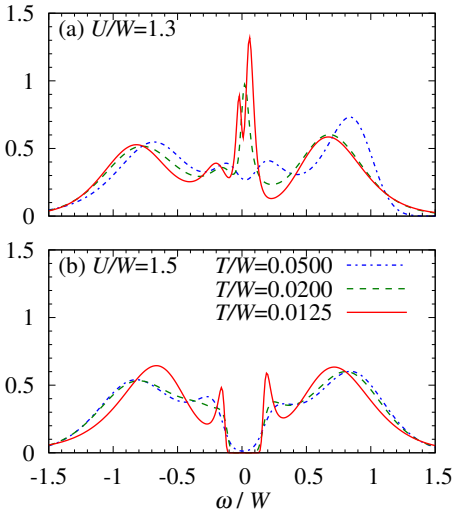

Fig. 7. (Color online) Temperature dependence of the density of states for $U/W = 1.3$ (a) and $U/W = 1.5$ (b).

low temperatures. This means that the coherence temperature T_0 characterizing quasiparticle formation is very low. This naturally gives rise to strong frustration and brings about unusual metallic properties near the Mott transition, as we will see momentarily below.

In order to clearly examine quasiparticle formation around the Mott transition, we compute the density of states (DOS), $-\frac{1}{\pi}\mathrm{Im}G_{\mathrm{loc}}(\omega + i0)$. This is calculated from the imaginary time single-electron Green's function $G_{\mathrm{loc}}(\tau) = -\langle \mathrm{T}_\tau c_{i\sigma}(\tau) c^\dagger_{i\sigma}(0)\rangle$ for real frequency ω by applying MEM. In Fig. 6, we show DOS at $T/W = 0.0125$ for several choices of the interaction strength U/W. At $U = 0$, DOS has three distinct energy bands including a δ-function peak above the Fermi level. As U/W increases, DOS forms heavy quasiparticle peaks around the Fermi level and finally develops a dip at $U/W \sim 1.40$, signaling the Mott transition. We find two characteristic properties in the metallic phase close to the transition point. First, the heavy quasiparticles survive up to the transition point ($U/W = 1.30$ and 1.36) and there is no evidence for pseudo-gap formation, in accordance with the U- and T-dependence of double occupancy in Fig. 4. This is related to the suppression of magnetic instabilities in our system, in contrast to the square lattice case, where quasiparticle dynamics are strongly incoherent and a pseudo gap opens. The second point is a large renormalization of quasiparticle weight near the transition point. We can see three renormalized peaks near the Fermi level: not only the peak near the Fermi surface but also the two other bands away from the Fermi surface are renormalized to participate in quasiparticle formation.

Such evolution of quasiparticles can be also clearly seen in the T-dependence of DOS shown in Fig. 7. In the insulating phase ($U/W = 1.5$), there is a dip struc-

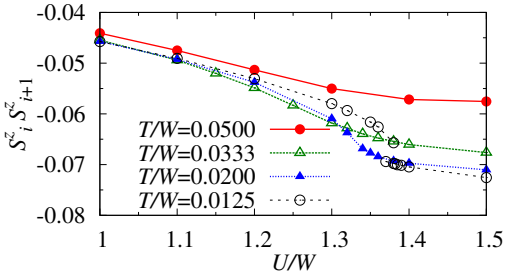

Fig. 8. (Color online) Nearest-neighbor spin correlation function $\langle S_i^z S_{i+1}^z \rangle$ as a function of U/W.

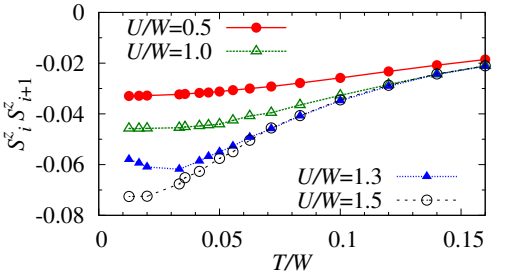

Fig. 9. (Color online) Temperature dependence of $\langle S_i^z S_{i+1}^z \rangle$ for several values of U/W.

ture near the Fermi level already at quite high temperatures and it becomes more prominent with lowering T, and eventually a gap opens at low temperatures. On the other hand, in the metallic phase close to the Mott transition ($U/W = 1.3$), the quasiparticle peak develops as T decreases instead of the pseudo-gap formation. The three quasiparticle peaks evolve near the Fermi level with lowering T, although there exists a dip instead of peak at high temperatures. Therefore, the three quasiparticle bands are all relevant for low-energy excitations near the Mott transition, in contrast to the weak coupling regime where only the single band around the Fermi surface is relevant.

3.2. *Anomalous spin correlations in the metallic phase*

It should be noted that quasiparticles exhibit anomalous spin correlations due to strong frustration around the transition point. We show the nearest-neighbor spin correlation function $\langle S_i^z S_{i+1}^z \rangle$ at several temperatures in Fig. 8. Here, $S_i^z = (c_{i\uparrow}^\dagger c_{i\uparrow} - c_{i\downarrow}^\dagger c_{i\downarrow})/2$. It is seen that $\langle S_i^z S_{i+1}^z \rangle$ is always negative so that the spin correlation is antiferromagnetic (AF), which gives rise to strong frustration on the kagomé lattice. With increasing U/W, the nearest-neighbor AF spin correlation is gradually enhanced. In the insulating phase the AF spin correlation becomes stronger as T decreases. We note that the low-temperature spin correlation in the insulating phase is weaker than that in isolated triangle, $\langle S_i^z S_{i+1}^z \rangle = -1/12$. More striking behavior appears in the metallic phase near the transition point: the AF spin correlation is once enhanced and then suppressed with decrease of temperature, as shown in Fig. 9. This anomalous temperature dependence comes from the competition between the quasiparticle formation and the frustrated spin correlations, which is characterized by two energy scales: the coherence temperature T_0 and T_M characterizing the AF spin fluctuations. The AF correlation enhanced around $T \sim T_M$ stabilizes localized moments and gives rise to frustration, which is consistent with the monotonic enhancement of spin correlations in the insulating phase in Fig. 9. On the other hand, when the system is in the metallic phase, electrons recover coherence in itinerant motion below T_0. Frustration is thus relaxed by itinerancy of electrons through the suppression of AF correlations at $T < T_0$. Therefore, the nonmonotonic temperature-dependence in $\langle S_i^z S_{i+1}^z \rangle$ demonstrates the formation of the heavy

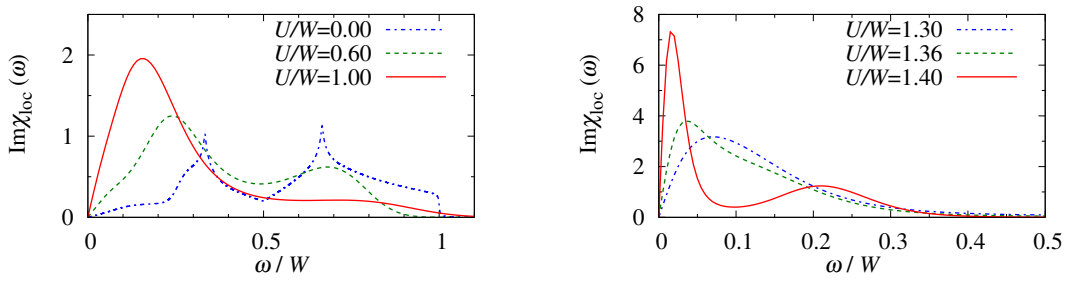

Fig. 10. (Color online) Dynamical susceptibility $\mathrm{Im}\chi_{\mathrm{loc}}(\omega)$ for several values of U/W at $T/W = 0.0125$.

quasiparticles under strong frustration effects.

We can see the anomalous properties also in dynamical spin correlations. We compute the dynamical spin susceptibility defined by

$$\chi_{\mathrm{loc}}(\omega) = i\int_0^\infty dt e^{i\omega t}\langle[S_i^z(t), S_i^z(0)]\rangle. \tag{3·2}$$

Shown in Fig. 10 is $\mathrm{Im}\chi_{\mathrm{loc}}(\omega)$ around the Mott transition at $T/W = 0.0125$. Note that $\mathrm{Im}\chi_{\mathrm{loc}}(\omega)$ dramatically changes its profile around the Mott transition. In the insulating phase ($U/W = 1.4$), there are two distinct peaks in $\mathrm{Im}\chi_{\mathrm{loc}}(\omega)$ at low energies. On the other hand, in the metallic phase ($U/W = 1.3$, 1.36), two peaks are renormalized into a single peak and its peak value is strongly suppressed. This is a clear demonstration of drastic change in spin dynamics between metallic and insulating phases in frustrated systems. The double-peak structure in the insulating phase is due to the dominant short-range AF correlations at low temperatures. The strongly enhanced low-energy peak in $\chi_{\mathrm{loc}}(\omega)$ corresponds to excitations among the almost degenerate states for which a singlet spin pair is formed inside the unit cell, while the higher-energy hump is caused by the excitations from these low-energy states to other excited states. In the metallic phase, the AF correlations are suppressed and then frustration is relaxed via the itinerancy of electrons, which leads to the renormalized single peak structure in $\chi_{\mathrm{loc}}(\omega)$. We can thus say that the dramatic change in $\chi_{\mathrm{loc}}(\omega)$ characterizes the competition between itinerancy and frustration of correlated electrons around the Mott transition.

3.3. *Enhanced one-dimensional spin correlations*

We now investigate how these local spin correlations affect long range correlations by calculating the **q**-dependence of static susceptibility,

$$\chi_{\gamma\delta}(\mathbf{q}) = \int_0^\beta d\tau \sum_{\mathbf{k},\mathbf{k}'} \left\langle c^\dagger_{\mathbf{k}\gamma\uparrow}(\tau)\, c_{\mathbf{k}+\mathbf{q}\gamma\downarrow}(\tau)\, c^\dagger_{\mathbf{k}'+\mathbf{q}\delta\downarrow}(0)\, c_{\mathbf{k}'\delta\uparrow}(0)\right\rangle, \tag{3·3}$$

where $\gamma, \delta = 1, 2, 3$ denote the superlattice indices. We compute $\chi_{\gamma\delta}(\mathbf{q})$, following the procedure explained in the previous section, where nearest-neighbor as well as local vertex corrections are included. Let us introduce $\chi_m(\mathbf{q})$ for three normal modes ($\chi_1(\mathbf{q}) > \chi_2(\mathbf{q}) > \chi_3(\mathbf{q})$) defined by eigenvalues of the 3×3 matrix $\chi_{\gamma\delta}(\mathbf{q})$. We show

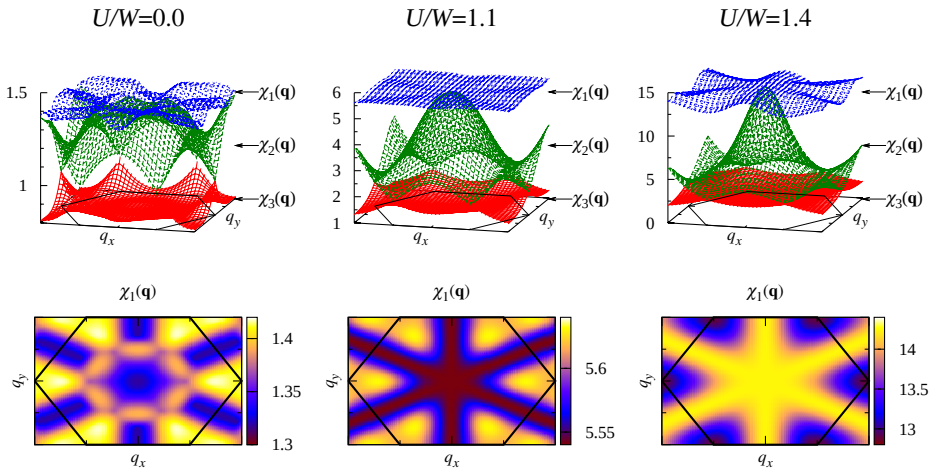

Fig. 11. Wave-vector dependence of the static susceptibility $\chi_m(\mathbf{q})$ for several values of U/W at $T/W = 0.0333$. The three-dimensional plots of $\chi_m(\mathbf{q})$ are shown in the upper panels, from top to bottom, $m = 1, 2, 3$. The two-dimensional plots in the lower panels show the dominant mode of the susceptibility $\chi_1(\mathbf{q})$ in the upper panels. Hexagons in figures denote the first Brillouin zone, as shown in Fig. 2(b).

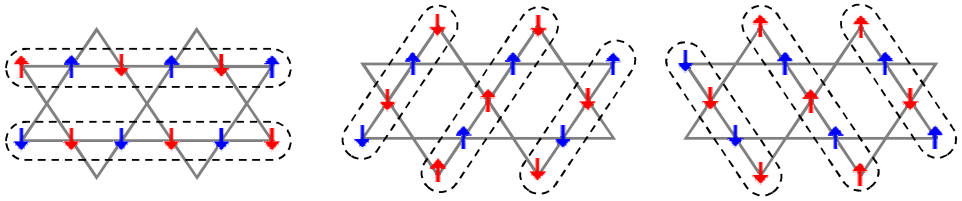

Fig. 12. (Color online) Enhanced 1D spin correlations in the insulating phase: $U/W = 1.4$ at $T/W = 0.0333$.

$\chi_m(\mathbf{q})$ for several choices of U/W at $T/W = 0.0333$ in Fig. 11. The maximum eigenvalue $\chi_1(\mathbf{q})$ has much weaker $\mathbf{q}$-dependence than that for the other two modes, while the second largest mode $\chi_2(\mathbf{q})$ has a strong $\mathbf{q}$-dependence with a maximum at $\mathbf{q} = (0, 0)$. We note that these results are in accordance with those obtained by FLEX[13] and also by QMC approaches.[14] However, we find more striking features in the strong coupling regime. At $U/W = 0$, $\chi_1(\mathbf{q})$ has a maximum at six points in the Brillouin zone. With increase of U/W, $\chi_1(\mathbf{q})$ is enhanced not only at the six points but also on the three lines through Γ and M points. Thus the $\mathbf{q}$-dependence of $\chi_1(\mathbf{q})$ becomes much flatter at $U/W = 1.1$ than in the $U = 0$ case. Once the system enters the insulating phase, the $\mathbf{q}$-dependence of $\chi_1(\mathbf{q})$ dramatically changes its character due to the enhancement of short range AF correlations. At $U/W = 1.4$, the susceptibility $\chi_1(\mathbf{q})$ further grows along the three lines in $\mathbf{q}$ space and becomes dominant there instead of the six points that give the leading magnetic mode in the weak coupling regime. Furthermore, the analysis of the eigenvectors of $\chi_1(\mathbf{q})$ concludes that two spins in the unit cell are antiferromagnetically coupled but the other spin is free. This implies that the enhanced spin fluctuations favor a spatial

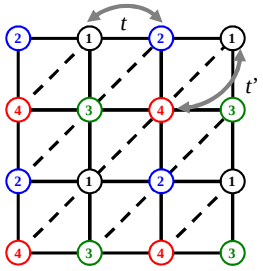

Fig. 13. (Color online) Sketch of the anisotropic triangular lattice

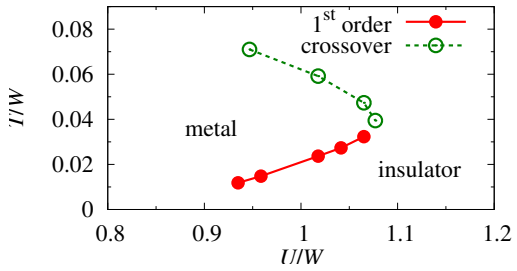

Fig. 14. (Color online) Phase diagram of Hubbard model on anisotropic triangular lattice for $t'/t = 0.8$.

spin configuration in which one-dimensional (1D) AF-correlated spin chains are independently formed across free spins in three distinct directions. We illustrate a schematic picture of the three equivalent types of enhanced spin correlations in Fig. 12. This is one of the naturally expected spin correlations on the kagomé lattice, since it stabilizes antiferromagnetic configurations in one direction, which is more stable than the naively expected spin configuration having a singlet pair and a free spin in each cluster. We wish to emphasize that the 1D correlations found here in the finite-temperature Mott insulating phase are different from those for the Heisenberg model on the Kagomé lattice with the nearest-neighbor exchange obtained by both classical and semi-classical approximations,[81),82)] but are similar to the $\mathbf{q} = 0$ structure predicted for the classical Heisenberg model with a further neighbor exchange.[81)] The essential difference is that there is almost no correlation between the different chains in our results for the Hubbard model. These 1D correlations have been recently studied by Udagawa and Motome by means of the larger-cluster CDMFT.[84)] They have clarified the origin of the 1D correlations in terms of the strong renormalization effects of electrons at finite temperatures.

Summarizing this section, we have clarified that the metallic phase is stabilized up to fairly large U in electrons on the strongly frustrated kagomé lattice, resulting in the three-band heavy quasiparticles. We have seen that this gives rise to several anomalous properties of spin correlation functions in the metallic phase close to the Mott transition point. As a characteristic of the kagomé lattice system, novel 1D spin correlations appear in the insulating phase at intermediate temperatures. With approaching zero temperature, the spin liquid state or other nonmagnetic ordered states are expected to be realized at low temperatures.[10),83)]

§4. Anisotropic triangular lattice system

In this section, we study the finite-temperature Mott transition in the Hubbard model on the anisotropic triangular lattice. We determine the U-T phase diagram as shown in Fig. 14, which shows a remarkable property, *i.e.* reentrant behavior in the Mott transition.

Let us consider the Hubbard model (2·1) on the anisotropic triangular lattice

shown in Fig. 13,

$$t_{ij} = \begin{cases} -t & (t>0) \quad (\text{site } i \text{ an } j: \text{ nearest neighbors}) \\ -t' & (t'>0) \quad (\text{site } i \text{ an } j: \text{ diagonal}) \\ 0 & \quad (\text{otherwise}) \end{cases} . \tag{4·1}$$

We use the band width W as an energy unit for given anisotropy t'/t, and it is $W = 4(t+t') + t^2/t'$ for $t' > 0.5t$ and $W = 8t$ for $t' < 0.5t$. To analyze this model, we use the four-site cluster CDMFT. Considering four sublattices labeled by 1-4, as shown in Fig. 13, we map the original lattice model to a four-site cluster model coupled to the self-consistently determined medium. Fifty-times iterations in a CDMFT procedure and typically 10^6 QMC sweeps with Trotter time slices $L = 12t\beta$ are performed to obtain numerical convergence.

4.1. *Mott transition*

We investigate the Mott transition for the model (2·1) at half filling. To this end, let us first compute the T-dependence of the double occupancy $D_{\text{occ.}} = \langle n_{i\uparrow} n_{i\downarrow} \rangle$ for typical interaction strength U/W, where the ground state is insulating and also in the vicinity of Mott transition point. We find a remarkable property in our frustrated system, *i.e.* nonmonotonic T-dependence of $D_{\text{occ.}}$. It is seen in Fig. 15 that $D_{\text{occ.}}$ decreases at high temperatures, and then exhibits an upturn in the intermediate temperature region having a local minimum at $T/W \sim 0.06$, as T decreases. At much lower temperatures, $D_{\text{occ.}}$ starts to decrease again and thus shows a hump structure. The nonmonotonic T-dependence of $D_{\text{occ.}}$ implies that our system once changes from insulating to metallic and then reenters the insulating phase as T decreases. This is quite different from that known for the infinite dimensional Hubbard model, where $D_{\text{occ.}}(T)$ has a single minimum at the Fermi-liquid coherence temperature T_0. In the latter model, the system is insulating at $T > T_0$ and Fermi liquid like at $T < T_0$.[29] The nonmonotonic behavior found here is also different from that for the unfrustrated square lattice Hubbard model. In the square-lattice Hubbard model, the Fermi-liquid coherence is disturbed by the antiferromagnetic (AF) interaction due to the perfect nesting of Fermi surface, which results in monotonic decrease of $D_{\text{occ.}}$.[68),79)] It is seen that the hump structure in $D_{\text{occ.}}$ becomes more prominent and shifts to lower temperatures as t' increases, although it is less visible for $t'/t = 0.5$.

We can see such characteristic behavior also in DOS as shown in Fig. 16. This is wave-vector-integrated electron spectral function. For $t'/t = 0.5$, DOS shows a dip structure near the Fermi level at high temperatures. As T decreases, the dip becomes prominent, and finally a gap opens clearly in the low-T insulating phase. On the other hand, for $t'/t = 0.8$ with stronger frustration, the nonmonotonic behavior appears in DOS. The quasiparticle peak develops near the Fermi level with lowering temperature, although the dip structure appears at high temperatures. As T further decreases, the quasiparticle peak disappears and an insulating gap opens again. These properties are consistent with the results of $D_{\text{occ.}}$. Therefore, it is concluded that the nonmonotonic behavior is a characteristic feature caused by geometrical frustration.

In order to clarify whether the change between metal and insulator is a real phase

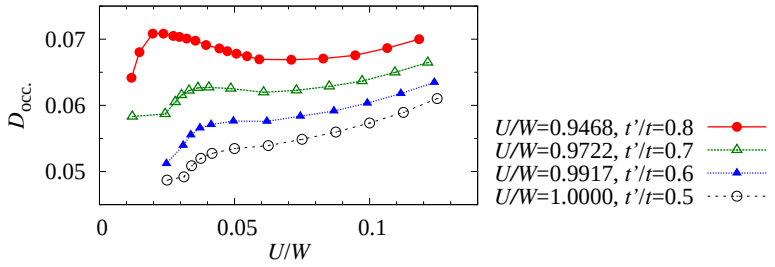

Fig. 15. (Color online) Nonmonotonic temperature dependence of double occupancy in the typical strong-U regime $U \sim W$, where ground states are insulating and in the vicinity of the Mott transition.

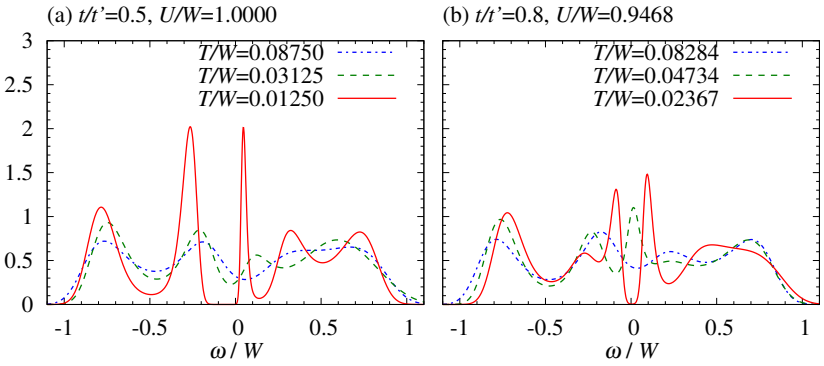

Fig. 16. (Color online) Temperature dependence of DOS for $t'/t = 0.5$ (a) and $t'/t = 0.8$ (b). For $t'/t = 0.8$, the metallic quasiparticle peak appears near the Fermi level at the intermediate temperature $T/W = 0.04734$.

transition or crossover, we examine the double occupancy for typical anisotropy $t'/t = 0.8$ with varying U. Let us start from the noninteracting system to reach the large-U regime, typically $U/W \sim 1.2$, and then calculate $D_{\rm occ.}$ with gradually decreasing U. It is seen in Fig. 17 that the double occupancy jumps at critical interaction strength U_c as U decreases, signaling a first-order Mott transition. The size of the jump shrinks as T increases, and eventually vanishes above $T/W \sim 0.035$. It is expected that the critical end point is located at $T/W \sim 0.035$ and $U/W \sim 1.077$. At high temperatures, the system exhibits a crossover between metal and insulator, where we define the boundary by the temperature at which the double occupancy takes the first local minimum at high temperatures, as seen in Fig. 15. Note that the metal-insulator boundary is in accordance with that determined by the local minimum of the density of states at the Fermi energy. We thus end up with the phase diagram shown in Fig. 14. We wish to emphasize here that $U_c(T)$ in our system has a slope with the opposite sign to the behavior in the infinite dimensional model at low temperatures, whereas the high-T crossover exhibits similar behavior to the infinite-dimensional case.

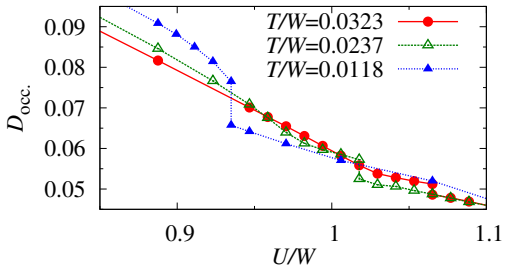

Fig. 17. (Color online) Double occupancy as a function of interaction strength U/t for $t'/t = 0.8$ at several temperatures. We show only the transition from insulator to metal with weakening U (defined as U_{c1}), although we find hysteresis.

4.2. *Reentrant behavior*

It is known that the single-site DMFT gives entropy of about $\ln 2$ per site in the paramagnetic insulating phase corresponding to localized free spins and smaller entropy is realized in the metallic phase with the Fermi-liquid coherence. Therefore, near the Mott transition temperature, the system is insulating at high temperatures to gain large entropy and the metallic phase exists always in the lower temperature region.[29] It should be noted, however, that the spatial fluctuations, which are not taken into account in the single-site DMFT, are important at low temperatures. For instance, according to the dynamical cluster study of the square-lattice Hubbard model, the Fermi-liquid metallic phase does not appear because of strong AF correlations.[68),79)] In contrast, the magnetic correlations in our system are hard to develop until low temperature $T/W \sim 0.05$ due to strong geometrical frustration. Hence, when the temperature is lowered, the entropy is released not by spin correlations but by the itinerancy of electrons at $T/W > 0.05$, which gives rise to the crossover behavior from insulator to metal as shown in Fig. 14. The emergence of such Fermi-liquid states is one of the characteristics in the vicinity of the Mott transition with geometrical frustration.[73] Note that the magnetic correlations are enhanced at much lower temperatures, finally triggering a first-order phase transition from the Fermi liquid to an insulator with smaller entropy. Hence with decreasing T, $U_c(T)$ decreases at low temperatures ($T/W < 0.05$) in contrast to the behavior at higher temperatures ($T/W > 0.05$). We can thus say that the reentrant Mott transition found here for the anisotropic triangular lattice is caused by the competition induced by geometrical frustration between the Fermi-liquid formation and the magnetic correlations.

Let us now discuss the momentum resolved single-electron spectrum $A_{\mathbf{k}}(\omega)$, in which we can clearly see the development of the quasiparticles and magnetic correlations discussed above. This is calculated by using Eq. (2·7) and MEM. We show $A_{\mathbf{k}}(\omega)$ for $U/W = 0.9468$, $t'/t = 0.8$ at typical temperatures in Fig. 18. It is seen that $A_{\mathbf{k}}(\omega)$ shows an insulating behavior at high temperatures, where it has a large Hubbard gap of order of U/W and no quasiparticle peak. With decreasing temperature, a quasiparticle peak starts to develop inside the gap, and results in a quasiparticle band with weak dispersion. This clearly suggests the appearance of

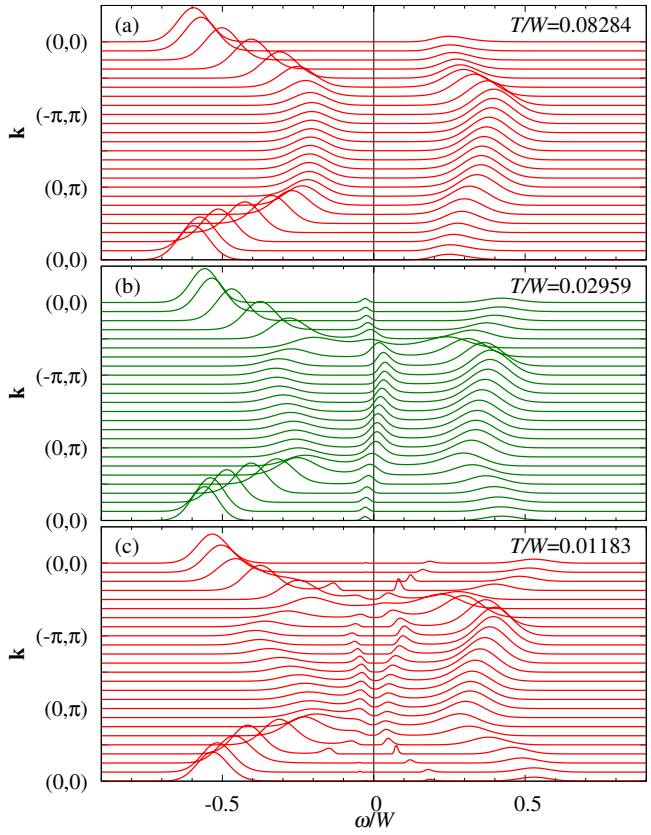

Fig. 18. (Color online) Momentum resolved single-electron spectrum $A_{\mathbf{k}}(\omega)$ for $U/W = 0.9468$, $t'/t = 0.8$ at several temperatures.

the frustration-induced metallic phase. The emergence of the metallic phase due to geometrical frustration is in accordance with the previous studies of the Hubbard model on the triangular lattice[18),68)] and the kagomé lattice.[73)] As temperature further decreases, the quasiparticle peaks split and acquire a very small gap, and the system enters another insulating phase again. Note that the small gap is caused by the exchange interaction among quasiparticles, which is consistent with the results of the CDMFT study with exact diagonalization method at zero temperature.[24)] It is thus confirmed that the present frustrated system exhibits the insulator-metal-insulator reentrant behavior with decreasing temperature.

4.3. *Magnetic instability*

Here, we wish to briefly discuss magnetic instability. The static spin susceptibility $\chi(\mathbf{q})$ computed for typical U/W and T/W around the Mott transition is shown in Fig. 19. For $t'/t < 0.7$ (weak frustration), it is seen that $\chi(\mathbf{q})$ develops a peak structure with lowering T at $\mathbf{q} = (\pi, \pi)$ corresponding to the commensurate antiferromagnetism. The behavior is consistent with recent studies of the Hubbard model around the Mott transition.[17),22),27)] Quite different tendency appears at

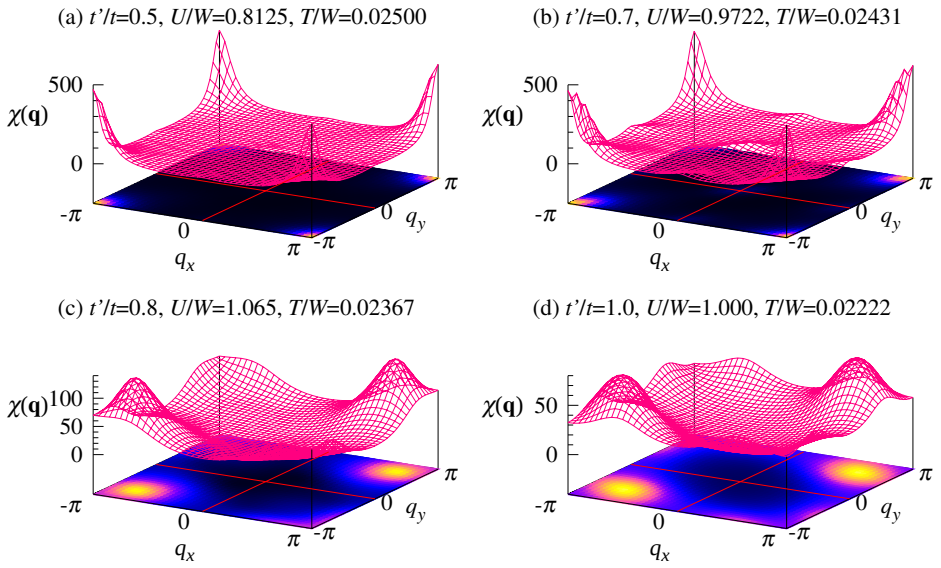

Fig. 19. Static spin susceptibility $\chi(\mathbf{q})$ around the Mott transition point.

$t'/t = 1.0$ (triangular lattice), where the spin susceptibility $\chi(\mathbf{q})$ has a maximum at $\mathbf{q} = (2\pi/3, 2\pi/3)$ corresponding to the 120° structure, and the development of $\chi(\mathbf{q})$ is much slower than the AF correlations for small t'. For $U/W = 1.065$, $t'/t = 0.8$ at $T/W = 0.02367$, where the system is in the insulating phase near the Mott transition point, $\chi(\mathbf{q})$ does not diverge, but takes a maximum at incommensurate wave vectors $\mathbf{q} \sim (0.7\pi, 0.7\pi)$. It is remarkable that $\chi(\mathbf{q})$ remains finite just below the first order Mott transition temperature and hence the paramagnetic Mott insulator is not precluded by the magnetically ordered phase. This is contrasted to the single-site DMFT results: the magnetic order conceals the Mott transition.[29),38)] On the other hand, the magnetic ordering in our case, which is strongly suppressed by frustration effects, emerges below the Mott transition temperature, although a finite-temperature magnetic transition is due to a mean-field type approximation. In this way, the magnetic correlations play a crucial role in driving the Mott transition at low temperatures, although they do not trigger a real magnetic instability.

4.4. *Controlling frustration*

It is to be noted that the determined phase diagram (Fig. 14) in the U-T plane for $t'/t = 0.8$ is qualitatively consistent with the experimental data[16)] in κ-(BEDT-TTF)$_2$Cu[N(CN)$_2$]Cl with $t'/t \sim 0.75$. Now, a question naturally arises: what happens if we control frustration by changing the ratio of t'/t. To this end, we have systematically studied the Mott transition for different choices of t'/t. For weakly frustrated case $t'/t \leq 0.5$, we have found that the Fermi-liquid formation is suppressed by the strong AF correlations, and thus the reentrant Mott transition becomes less prominent. In this case, the Mott transition temperature is very low[85)] and the AF long range order hides the Mott transition within CDMFT approach.

For fully frustrated case $t' \sim t$, on the other hand, the Fermi-liquid states are well stabilized by frustration and the metallic region is extended, because the magnetic fluctuations of the 120° structure are weak. We thus expect that the low-temperature Mott transition line shifts to lower-temperature regime.[21] Note that the above tendency is consistent with the experiments on another organic material κ-(BEDT-TTF)$_2$Cu$_2$(CN)$_3$ with $t' \sim t$,[7] where any magnetic order was not observed so far experimentally. We conclude that the reentrant behavior can be observed most clearly in electron systems with moderate frustration.

Summarizing this section, we have found novel reentrant behavior in the Mott transition in the anisotropic triangular lattice Hubbard model, and have clarified that the reentrant behavior in the Mott transition is caused by the competition between the Fermi-liquid formation and the magnetic correlations under geometrical frustration.

§5. Summary

We have studied the Hubbard model on the kagomé and anisotropic triangular lattice by means of the cellular dynamical mean field theory. Through the systematic studies, we have elucidated some characteristic properties common to frustrated electron systems near the Mott transition. First, we have shown that the metallic phase is stabilized up to fairly large Hubbard interactions under strong frustration in both models. This naturally leads to the formation of strongly renormalized heavy fermions near the Mott transition point, where some anomalous properties are caused by almost localized electrons with strong geometrical frustration. One of such anomalous features emerges in the nonmonotonic temperature dependence of the spin correlation function found for the kagomé lattice model around the Mott transition. This is indeed due to electron correlations strongly influenced by frustration. We have also found that such anomalous spin correlations result in more striking behavior in the Mott transition in the case of the anisotropic triangular lattice system. Namely, the Mott transition shows novel reentrant behavior due to the competition between Fermi-liquid formation and magnetic correlations, as typically seen for the triangular lattice system for $t'/t = 0.8$.

Although we have used the small-cluster CDMFT in this paper, we believe that the anomalous properties found here for the Mott transition are robust, which may not qualitatively change even for a larger cluster size, since the competition between the Fermi-liquid formation and magnetic correlations should occur generally in frustrated electron systems, Therefore, we expect that nonmonotonic temperature dependence of the spin correlation function and/or the reentrant behavior in the Mott transition will be observed experimentally in a variety of frustrated electron systems.

Acknowledgment

We are deeply indebted to our collaborators in this field, K. Inaba, A. Koga, Y. Motome, S. Suga and have benefited from helpful discussions with T. Koretsune,

M. Udagawa, R. Arita, S. Onoda, and M. Imada. Discussions during the YITP workshop YKIS2007 on "Interaction and Nanostructural Effects in Low-Dimensional Systemsh were useful to complete this work. This work was partly supported by Grants-in-Aid for Scientific Research (No. 17071011, No. 19052003, No. 20029013, No. 19014013 and No. 19840031) and also by the Next Generation Supercomputing Project, Nanoscience Program, from the Ministry of Education, Sports, Science and Culture of Japan. A part of numerical computations was done at the Supercomputer Center at the Institute for Solid State Physics, University of Tokyo and Yukawa Institute Computer Facility.

References

1) S. Kondo *et al.*, Phys. Rev. Lett. **78**, 3729 (1997).
2) P. E. Jönsson, K. Takenaka, S. Niitaka, T. Sasagawa, S. Sugai, and H. Takagi, Phys. Rev. Lett. **99**, 167402 (2007).
3) K. Takada, H. Sakurai, E. Takayama-Muromachi, F. Izumi, R. A. Dilaian, and T. Sasaki, Nature (London) **422**, 53 (2003).
4) S Yonezawa, Y Muraoka, Y Matsushita and Z Hiroi, J. Phys.: Cond. Matt. **16**, L9 (2004).
5) S. Yonezawa, Y. Muraoka, Y. Matsushita, and Z. Hiroi, J. Phys. Soc. Jpn. **73**, 819 (2004).
6) S. Yonezawa, Y. Muraoka, Y. Matsushita, and Z. Hiroi, J. Phys. Soc. Jpn. **73**, 1655 (2004).
7) Y. Shimizu, K. Miyagawa, K. Kanoda, M. Maesato, and G. Saito, Phys. Rev. Lett. **91**, 107001 (2003).
8) S. Nakatsuji, Y. Machida, Y. Maeno, T. Tayama, T. Sakakibara, J. van Duijn, L. Balicas, J. N. Millican, R. T. Macaluso, and Julia Y. Chan, Phys. Rev. Lett. **96**, 087204 (2006).
9) Y. Okamoto, M. Nohara, H. Aruga-Katori, and H. Takagi, Phys. Rev. Lett. **99**, 137207 (2007).
10) G. Misguich and C. Lhuillier, *Frustrated Spin Systems*, edited by H. T. Diep (World Scientific, Singapore, 2004), and references therein.
11) M. P. Shores, E. A. Nytko, B. M. Bartlett, and D. G. Nocera, J. Am. Chem. Soc. **127**, 13462 (2005).
12) W. Koshibae and S. Maekawa, Phys. Rev. Lett. **91**, 257003 (2003).
13) Y. Imai, N. Kawakami, and H. Tsunetsugu, Phys. Rev. B **68**, 195103 (2003).
14) N. Bulut, W. Koshibae, and S. Maekawa, Phys. Rev. Lett. **95**, 037001 (2005).
15) S. Lefebvre, P. Wzietek, S. Brown, C. Bourbonnais, D. Jérome, C. Mézière, M. Fourmigué, and P. Batail, Phys. Rev. Lett. **85**, 5420 (2000).
16) F. Kagawa, T. Itou, K. Miyagawa, and K. Kanoda, Phys. Rev. B **69**, 064511 (2004).
17) T. Kashima, and M. Imada, J. Phys. Soc. Jpn. **70**, 3052 (2001).
18) Y. Imai and N. Kawakami, Phys. Rev. B **65**, 233103 (2002).
19) S. Onoda and M. Imada, Phys. Rev. B **67**, R161102 (2003).
20) S. Onoda and N. Nagaosa, J. Phys. Soc. Jpn. **72**, 2445 (2003).
21) O. Parcollet, G. Biroli, and G. Kotliar, Phys. Rev. Lett. **92**, 226402 (2004).
22) H. Yokoyama M. Ogata, and Y. Tanaka, J. Phys. Soc. Jpn. **75**, 114706 (2006).
23) T. Mizusaki, and M. Imada, Phys. Rev. B **74**, 014421 (2006).
24) B. Kyung, and A.-M. S. Tremblay, Phys. Rev. Lett. **97**, 046402 (2006).
25) B. Kyung, Phys. Rev. B **75**, 033102 (2007).
26) S. S. Kancharla and E. Dagotto, Phys. Rev. Lett. **98**, 016402 (2007).
27) T. Koretsune, Y. Motome and A. Furusaki, J. Phys. Soc. Jpn. **76**, 074719 (2007).
28) W. Metzner and D. Vollhardt, Phys. Rev. Lett. **64**, 324 (1989).
29) A. Georges, G. Kotliar, W. Krauth and M. J. Rozenberg, Rev. Mod. Phys. **68**, 13 (1996).
30) G. Kotliar, S. Y. Savrasov, K. Haule, V. S. Oudovenko, O. Parcollet, and C. A. Marianetti, Rev. Mod. Phys. **78**, 865 (2006).
31) M. Imada, A. Fujimori, and Y. Tokura, Rev. Mod. Phys. **70**, 1039 (1998).
32) R. Bulla, Phys. Rev. Lett. **83**, 136 (1999).
33) M. Jarrell, Phys. Rev. Lett. **69**, 168 (1992).
34) M. J. Rozenberg, Phys. Rev. B **52**, 7369 (1995).
35) T. Momoi, and K. Kubo, Phys. Rev. B **58**, 567 (1998).

36) Q. Si, S. Rabello, K. Ingersent and J. L. Smith, Nature (London) **413**, 804 (2001).
37) P. Sun and G. Kotliar, Phys. Rev. Lett. **91**, 037209 (2003).
38) R. Zitzler, N.-H. Tong, Th. Pruschke, and R. Bulla, Phys. Rev. Lett. **93**, 016406 (2004).
39) S. Sakai, R. Arita, and H. Aoki, Phys. Rev. Lett. **99**, 216402 (2007).
40) M. Jarrell, H. Akhlaghpour, and Th. Pruschke, Phys. Rev. Lett. **70**, 1670 (1993).
41) T. Mutou and D. Hirashima, J. Phys. Soc. Jpn. **63**, 4475 (1994).
42) T. Saso and M. Itoh, Phys. Rev. B **53**, 6877 (1996).
43) T. Ohashi, A. Koga, S. Suga, and N. Kawakami, Phys. Rev. B **70**, 245104 (2004).
44) T. Ohashi, S. Suga, and N. Kawakami, J. Phys. Condens. Matter **17**, 4547 (2005).
45) R. Arita, K. Held, A. V. Lukoyanov, and V. I. Anisimov, Phys. Rev. Lett. **98**, 166402 (2007).
46) J. E. Han, M. Jarrell, and D. L. Cox, Phys. Rev. B **58**, R4199 (1998).
47) S. Florens, A. Georges, G. Kotliar, and O. Parcollet, Phys. Rev. B **66**, 205102 (2002).
48) A. Koga, Y. Imai, and N. Kawakami, Phys. Rev. B **66**, 165107 (2002).
49) A. Koga, N. Kawakami, T.M. Rice, and M. Sigrist, Phys. Rev. Lett. **92**, 216402 (2004).
50) R. Sato, T. Ohashi, A. Koga, and N. Kawakami, J. Phys. Soc. Jpn. **73**, 1864 (2004).
51) L. de' Medici, A. Georges, G. Kotliar, and S. Biermann, Phys. Rev. Lett. **95**, 066402 (2005).
52) R. Arita and K. Held, Phys. Rev. B **72**, 201102 (2005).
53) A. Koga, K. Inaba, and N. Kawakami, Prog. Theor. Phys. Suppl. **160**, 253 (2005).
54) K. Inaba and A. Koga, J. Phys. Soc. Jpn. **76**, 094712 (2007).
55) R. W. Helmes, T. A. Costi, and A. Rosch, Phys. Rev. Lett. **100**, 056403 (2008).
56) I. Titvinidze, M. Snoek, and W. Hofstetter, Phys. Rev. Lett. **100**, 100401 (2008).
57) T. Higashiyama, K. Inaba, S. Suga, Phys. Rev. A **77**, 043624 (2008).
58) A. Koga, T. Higashiyama, K. Inaba, S. Suga, and N. Kawakami, J. Phys. Soc. Jpn. **77**, 073602 (2008).
59) M. Potthoff and W. Nolting, Phys. Rev. B **59**, 2549 (1999).
60) S. Okamoto and A. J. Millis, Phys. Rev. B **70**, 241104(R) (2004); Nature **428**, 630 (2004).
61) J. K. Freericks, *Transport in Multilayered Nanostructures: the Dynamical Mean-field Theory Approach* (Imperial College, London, 2006), and references therein.
62) Y. Tomio and T. Ogawa, J. Luminesci. **112**, 220 (2005).
63) T. Ogawa, Y. Tomio, and K. Asano, J. Phys.: Condens. Matter **19**, 295205 (2007).
64) M. H. Hettler, A. N. Tahvildar-Zadeh, M. Jarrell, T. Pruschke, and H. R. Krishnamurthy, Phys. Rev. B **58**, R7475 (1998).
65) A. I. Lichtenstein, and M. I. Katsnelson, Phys. Rev. B **62**, R9283 (2000).
66) G. Kotliar, S. Y. Savrasov, G. Pálsson, and G. Biroli, Phys. Rev. Lett. **87**, 186401 (2001).
67) S. Okamoto, A. J. Millis, H. Monien, and A. Fuhrmann, Phys. Rev. B **68**, 195121 (2003).
68) T. Maier, M. Jarrell, T. Pruschke, and M. H. Hettler, Rev. Mod. Phys. **77**, 1027 (2005).
69) B. Kyung, G. Kotliar, and A.-M. S. Tremblay, Phys. Rev. B **73**, 205106 (2006).
70) M. Potthoff, Eur. Phys. J. B **32**, 429 (2003); ibid. **36**, 335 (2003).
71) A. Toschi, A. A. Katanin, and K. Held, Phys. Rev. B **75**, 045118 (2007).
72) A. N. Rubtsov, M. I. Katsnelson, and A. I. Lichtenstein, Phys. Rev. B **77**, 033101 (2008).
73) T. Ohashi, N. Kawakami, and H. Tsunetsugu, Phys. Rev. Lett. **97**, 066401 (2006).
74) T. Ohashi, S. Suga, N. Kawakami, and H. Tsunetsugu, J. Phys.: Condens. Matter, **19**, 145251 (2007).
75) T. Ohashi, S. Suga, N. Kawakami, and H. Tsunetsugu, J. Mag. Mag. Mat., **310**, 879 (2007).
76) T. Ohashi, T. Momoi, H. Tsunetsugu, and N. Kawakami, Phys. Rev. Lett. **100**, 076402 (2008).
77) J. E. Hirsch, and R. M. Fye, Phys. Rev. Lett. **56**, 2521 (1986).
78) V. S. Oudovenko and G. Kotliar, Phys. Rev. B **65**, 075102 (2002).
79) S. Moukouri and M. Jarrell, Phys. Rev. Lett. **87**, 167010, (2001).
80) M. Jarrell and J. E. Gubernatis, Phys. Rep. **269**, 133 (1996).
81) A. B. Harris, C. Kallin, and A. J. Berlinsky, Phys. Rev. B **45**, 2899 (1992).
82) A. Chubukov, Phys. Rev. Lett. **69**, 832 (1992).
83) R. Budnik and A. Auerbach, Phys. Rev. Lett. **93**, 187205 (2004).
84) M. Udagawa and Y. Motome, unpublished.
85) H. Park, K. Haule, and G. Kotliar, arXiv:0803.1324.